PCCP

Accepted Manuscript

ROYAL SOCIETY OF CHEMISTRY

www.rsc.org/pccp

Liquid phase exfoliation and crumpling of inorganic nanosheets

Rozana Bari,[1] Dorsa Parviz,[2] Fardin Khabaz,[1] Christopher D. Klaassen,[1] Shane D. Metzler,[1] Matthew J. Hansen,[1] Rajesh Khare,[1] Micah J. Green[2,]*

[1]Department of Chemical Engineering, Texas Tech University, Lubbock, Texas 79409, USA

[2]Artie McFerrin Department of Chemical Engineering, Texas A&M University, College Station, Texas 77843, USA

**Corresponding author: micah.green@tamu.edu*

Abstract

Here we demonstrate through experiment and simulation the polymer-assisted dispersion of inorganic 2D layered nanomaterials such as boron nitride nanosheets (BNNSs), molybdenum disulfide nanosheets (MoS_2), and tungsten disulfide nanosheets (WS_2), and we show that spray drying can be used to alter such nanosheets into a crumpled morphology. Our data indicate that polyvinylpyrrolidone (PVP) can act as a dispersant for the inorganic 2D layered nanomaterials in water and a range of organic solvents; the effectiveness of our dispersion process was characterized by UV-vis spectroscopy, microscopy and dynamic light scattering. Molecular dynamics simulations confirm that PVP readily physisorbs to BNNS surfaces. Collectively, these results indicate that PVP acts as a general dispersant for nanosheets. Finally, a rapid spray drying technique was utilized to convert these 2D dispersed nanosheets into 3D crumpled nanosheets; this is the first report of 3D crumpled inorganic nanosheets of any kind. Electron microscopy images confirm that the crumpled nanosheets (1-2 μm in diameter) show a distinctive morphology with dimples on the surface as opposed to a wrinkled, compressed surface, which matches earlier simulation results. These results demonstrate the possibility of scalable production of inorganic nanosheets with tailored morphology.

1. Introduction

The emergence of graphene in the scientific literature has prompted new investigations of inorganic 2D nanosheets whose structure is analogous to graphene. Layered inorganic materials were first described by Tenne and coworkers in 1992; these materials include boron nitride nanosheets (BNNSs), molybdenum disulfide (MoS_2), and tungsten disulfide (WS_2).[1-4] In BNNSs, alternating B and N atoms form a planar structure resembling that of graphene.[5] MoS_2 and WS_2 nanosheets consist of a metallic layer sandwiched between two sulfur layers. Similar to graphene, the nanosheets layers are stacked together by weak van der Waals forces.[5,6]

These inorganic nanosheets possess an unusual combination of properties. Due to ionic bonding, BNNSs are electrically insulating, with a large electronic band gap (~4-6 eV),[3,7] but are also thermally conductive (2000 W m^{-1} K^{-1}) and mechanically strong,[8,9] These properties are ideal for thermal management of high-power electronics.[10] Additionally, BNNSs are resistant to oxidation and are chemically stable.[8,9] WS_2 and MoS_2 nanosheets possess strikingly different optical and electrical properties than their bulk form; this allows for novel applications in nanoelectronics and optoelectronics.[13] For example, MoS_2 and WS_2 nanosheets are semiconducting, with a direct electronic band gap of ~1.9 eV and ~2.1 eV, respectively,[50,51] in contrast to the bulk indirect band gap of 1.2 eV and 1.3 eV.[11,12] Since these materials exhibit direct band gap behavior, they have strong photoluminescence[13,14] and spin polarization.[15] These materials are also suitable for photovoltaics since absorber materials in thin film solar cells can be made from these inorganic layered materials.[16]

The isolation of these inorganic 2D nanosheets from the bulk material can be carried out via liquid-phase exfoliation.[17-19] In fact, the liquid-phase processing route is useful for

applications such as nanocomposites and electronic device deposition. Similar to graphene, prior reports on inorganic nanosheets in liquids have attempted both (1) direct (stabilizer-free) dispersion and (2) stabilizer-enabled dispersion. Inorganic nanosheet dispersions in organic solvents without stabilizers have been reported; however, the process requires extensive sonication and yields a comparatively low concentration of nanosheets.[18,20,21] Coleman and coworkers reported exfoliation of BNNSs in isopropanol (IPA), as well as MoS_2 and WS_2 in N-methyl-2-pyrrolidone (NMP).[18] For aqueous dispersions, surfactants and bile salts have been utilized to disperse BNNSs and MoS_2 nanosheets.[19]

Our current study focuses on the use of polyvinylpyrrolidone (PVP) as a dispersant for a broad class of 2D layered nanosheets (BNNSs, MoS_2, and WS_2). Our prior work showed that PVP can be used to disperse graphene in a wide range of solvents, [22] and our new data show that this technique is applicable to inorganic nanosheets as well. However, we should note that the recent, similar work of Guardia *et al.*[17] was concurrent with our own; their report similarly includes the dispersion of these nanosheets in water (but no other solvents) using PVP. Their report also indicates abnormally high nanosheet concentrations, likely due to insufficient centrifugation. Another recent publication by Ma *et al.* reported stabilization of BNNSs in chloroform at low concentrations with PVP and polythiophene dispersants and bath sonication.[23]

Molecular simulations have the ability to explicitly account for the specific chemical interactions in nanoscale systems. Despite the widespread interest in nanosheet dispersion, there have been relatively few quantum and molecular simulations of non-covalent interactions between boron nitride nanosheets (BNNS) or nanotubes (BNNT) and organic adsorbents.[24-28] In one prior study of particular interest,[25] attractive interactions between oligomers of three

polymers and BNNT were studied by simulations in the absence of any solvent medium. In this work, we utilized molecular dynamics (MD) simulations to investigate non-covalent interactions between PVP and an isolated boron nitride nanosheet in a medium of water.

In the current paper, we describe three novel advances in the area of inorganic nanosheet dispersion. (1) We demonstrate dispersion of these nanosheets in not only water but also a wide range of organic solvents. These results suggest that dispersion methods originally developed for graphene can straightforwardly be extended to other nanosheet types. (2) The experimental observation of PVP-assisted dispersion of BNNSs in solvents can be explained by hypothesizing that the PVP molecules physisorb on the individual BNNSs, thus shielding the nanosheet surface from water. In order to test this hypothesis, we carried out molecular simulations of the PVP-BNNS-water system.[25] The use of atomistically detailed models allows us to explicitly account for the specific molecular interactions in the system. Our simulation strategy consists of molecular dynamics simulation of the system where the PVP molecule is initially placed at long enough distances from the BNNS such that the two either have very weak direct interactions or do not directly interact with each other, and observing if it attaches to the BNNS surface during the course of the simulation. (3) Finally, we demonstrate that these 2D nanosheets can be converted to crumpled 3D nanostructures during spray drying. Prior work had demonstrated that colloidal graphene oxide dispersions can be manipulated to yield a crumpled morphology through aerosolization and rapid evaporation. This was applied to graphene oxide dispersions in a tube furnace; as the aerosolized droplets evaporate and shrink, surface tension compacts the GO to induce a highly wrinkled structure.[29-32] These crumpled graphene oxide nanosheets are aggregation-and compression-resistant in the solid state.[29,31] Our (Green) group recently showed that this spray drying process can be extended to crumpled pristine graphene using a simple

industrial spray drying technique.[33] In the current paper, we show that this spray drying technique for crumpling graphene can be generalized to other nanosheet types. To our knowledge, this is the first report of crumpled inorganic nanosheets and may open novel application areas for these materials.

2. Methods

2.1. Materials

Hexagonal boron nitride (hBN), molybdenum disulfide (MoS_2) and polyvinylpyrrolidone (PVP) (MW 10,000 g/mol) were purchased from Sigma Aldrich. Tungsten disulfide (WS_2) was brought from Santa Cruz Biotechnology. Another type of hBN was purchased from Industrial Supply Inc. The hBN from Sigma Aldrich (which we designate as hBN-I) has smaller flake size than the other (hBN- II). The average size of hBN-I is ~1 μm and large flake is ~3 μm. The organic solvents methanol, ethanol, isopropanol, chloroform, dimethylformamide (DMF), dimethyl sulfoxide (DMSO), and N-methyl-2-pyrrolidone (NMP) were purchased from Sigma Aldrich. All materials were used as received without any further purification.

2.2 Preparation of layered material dispersions

Stable aqueous dispersions of nanomaterials were prepared using PVP as a dispersant. PVP (10 mg mL^{-1}) was dissolved in water by magnetic stirring. 20 mg mL^{-1} of parent material was added to this solution, which was then tip sonicated in a water bath using a Misonix sonicator (XL 2000) at output wattage of 10 W for an hour. To remove large aggregates, the dispersions were centrifuged (Centrific Centrifuge 225, Fischer Scientific) for 4 hours at ~5000 rpm. The supernatant was collected and the absorbance was measured by a Shimadzu UV-vis

spectrophotometer 2550 at wavelengths of 200 nm to 800 nm. The supernatant concentration was measured by both vacuum filtration and absorbance measurements. The dispersions were vacuum filtered through Teflon filter paper (Millipore, 0.2 μm) and dried overnight. The weight of the filter paper was measured before and after filtration, and the dispersed nanomaterial concentration was determined from the weight difference. A PVP solution in water (10 mg mL^{-1}) was used as a blank to eliminate the background effect. The Lambert-Beer law ($A = \alpha LC$, where α is the extinction coefficient, A is the absorbance, C is the concentration, and L is the path length) was utilized to calculate α. The absorbance A is proportional to the product of concentration C and path length L. The absorbance spectra of the PVP-stabilized nanomaterial dispersions and the plots of absorbance vs. concentration are shown in Figure S1. The absorbance spectra for BNNSs, MoS_2, and WS_2 are plotted in Figure S1a, Figure S1c, and Figure S1e, respectively. The values of α were determined to be 1.1 x 10^3 mL mg^{-1} m^{-1} for BNNSs at 350 nm (Figure S1b), 5.2 x 10^2 mL mg^{-1} m^{-1} for MoS_2 at 674 nm (Figure S1d), and 4.2 x 10^2 mL mg^{-1} m^{-1} for WS_2 at 630 nm (Figure S1f), respectively. The values of the extinction coefficient are of the same order of magnitude with the extinction coefficient with other systems reported by Guardia *et al*.[17] The same procedure was followed to make nanosheet dispersions in methanol, ethanol, isopropanol, choloroform, DMF, DMSO, and NMP. In the case of the organic solvents the sonication was performed in ice-water bath to prevent evaporation of the solvent.

2.3. Dispersion Characterization

The dispersion quality of PVP-stabilized nanomaterials in water was investigated by high resolution transmission electron microscopy (HRTEM) in a Hitachi H8100 electron microscope.

Multiple droplets of the dispersions were placed onto holey carbon grids, which were then air dried. A voltage of 75 kV was used to image the specimens.

PVP-stabilized nanomaterial dispersions were frozen in a freezer at -20°C and dried in a freeze-dryer (Vitris Benchtop Freeze Dryer) overnight to yield dry powdered samples. The freeze-dried samples were redispersed in water without sonication. These samples were centrifuged, and the recovered concentration of dispersed nanosheets was calculated from the absorbance values.

The morphology of the powdered nanomaterial samples was observed in a HITACHI S-4300 electron microscope at an accelerating voltage of 10 kV and a working distance of 8 mm. Scanning electron microscope (SEM) samples were prepared by sputter coating with Au/Pd in a Hummer V Technics sputter coater at 10 kV and 10 mA current for 1 minute at a rate of 10 nm/min.

The particle size distribution of the nanomaterials was determined at room temperature using dynamic light scattering by a Zetatrac analyzer from Microtrac Inc.

PVP-stabilized nanomaterial dispersions were processed in a spray dryer (Buchi 290 mini spray dryer) to yield crumpled nanosheets. The operating temperature and pressure was 220°C and 60 psi respectively.

2.4. Simulation Methods

The PVP-BNNS-water system is simulated in a cubic box containing 75162 atoms. The BNNS sheet of size 50 Å × 50 Å is placed inside a cubic box of edge length 92 Å. A long polymer chain containing *80* monomers of polyvinylpyrrolidone (PVP) was introduced in the box; the PVP and the BNNS molecules were solvated using water. The BNNS sheet is modeled using the

three-body Tersoff potential[34] while TIP3P model parameters are employed for water molecules.[35] The SHAKE algorithm[36] was used to constraint the OH bond length of the water molecules. The general AMBER force field[37,38] is used to treat the interactions between the PVP molecule and water atoms, and the Lennard-Jones (LJ) interaction between the BNNS[39] and water as well as *PVP* is calculated based on the Lorentz-Berthelot mixing rules similar to the previous simulation work.[24] The partial charges on PVP atoms were computed by the AM1-BCC method,[40,41] while those for BNNS atoms were taken from literature.[42] A cut-off distance of 12 *Å* is used for van der Waals and Coulombic interactions. Tail correction and particle-particle particle-mesh algorithm (PPPM) are employed for calculating the long range interactions.[43] The temperature and pressure of the system are held constant at T = 300 *K* and P = 1 *atm* by applying Nosé-Hoover[44] thermostat and barostat, respectively. All molecular simulations are performed by using the LAMMPS[45] simulation package. A time step of 1 *fs* is used in all of the simulations.

Initial configuration of PVP-BNNS-water systems: Three different simulations were carried out to test the interaction between the PVP molecules and the BNNSs in water. The BNNS was first placed parallel to the *xy* plane in the simulation box. Three different system configurations were then created by placing the PVP molecule in the *xy* plane such that it was at center of mass distance = 10 *Å,* 20 *Å* and 35 *Å* from the BNNSs. For this purpose, the PVP molecule was placed parallel to the BNNSs (see Figure 1a). Thus, although, for example, in the third case, while the center of mass distance between the BNNS and the PVP molecules was fixed at 35 *Å*, the shortest distance between any atom of the PVP molecule and the BNNS was 33.4 *Å*. Water molecules were then added to the simulation box. Figure 1 shows the initial conformation of the molecules in the system. The system configuration was then equilibrated using a constant *NVT*

(constant number of molecules, volume and temperature) simulation followed by an additional constant *NPT* (constant number of molecules, pressure and temperature) simulation of 2 *ns* duration. We note that the positions of the BNNSs and the PVP atoms were fixed by applying harmonic constraints during the equilibration stage whereas water molecules were allowed to move freely in the system. These harmonic constraints were released after the equilibration stage and the constant *NPT* MD simulation production run was carried out for the duration of 25 *ns* for each of the three systems.

3. Results and discussion

3.1. Nanosheet dispersion

Our previous report showed that PVP acts as an effective dispersant for graphene both in water and various organic solvents.[22] Here we demonstrate that this same technique is applicable to a wide range of inorganic nanosheets as well, including boron nitride (BN), molybdenum disulfide (MoS_2), and tungsten disulfide (WS_2).[46-48] This was initially surprising because these results suggest that appears that the PVP-nanosheet interactions are independent of nanosheet surface chemistry.

Figure 2 shows PVP-stabilized aqueous dispersions of BNNSs, MoS_2, and WS_2 nanosheets. The dispersions were prepared by tip sonicating the parent materials in a PVP solution; subsequent centrifugation was performed to remove large aggregates. The supernatant was collected, and the absorbance was measured by a UV-vis spectrophotometer. The dispersed nanosheet concentrations were gravimetrically obtained by vacuum filtering the dispersions and washing the resulting film. The relationship between concentration and absorbance is shown in

detail in the supporting information for each of the nanosheet types (Figure S1). We used a 635 nm laser light to confirm the Tyndall effect to directly probe these colloidal dispersions; Figure 3 shows the Tyndall effect on BNNSs (Figure 3a), MoS_2 (Figure 3b), and WS_2 (Figure 3c).. The light scattering effect is visible when the colloidal nanoparticle size is below or near the wavelength of the light.[49]

In order to compare the pre-exfoliation and post-exfoliation morphology, we examined the parent material structure. The parent materials are initially compact and flat as shown in the SEM images (Figure 4). The typical flake size of parent hBN-I powder (Figure 4) is the smallest (~1 μm) compared to MoS_2 and WS_2. The apparent lateral size of parent MoS_2 and WS_2 is ~2 μm (Figure 4b) and ~3 μm (Figure 4c), respectively. The magnified view of parent hBN flakes (inset of Figure 4a) shows an oval shaped morphology whereas MoS_2 flakes are irregularly shaped with rough edges (inset of Figure 4b), and WS_2 flakes are also irregularly shaped with straight, smooth edges (inset Figure 4c).

TEM was performed on the nanosheet dispersions to determine lateral size, morphology, and the number of nanosheet layers (Figure 5); additional TEM images are available in supporting information in Figure S2. Most of the BNNSs exhibit smooth, curved edges with an overall oval shape; the typical size of the nanosheets is ~700 nm (Figure 5a). The TEM images of the BNNSs are similar to others depicted in recent studies on BN exfoliation.[50,51] The smooth shape associated of the dispersed BNNSs is quite unusual compared with the irregular complex shapes seen in dispersed graphene. The similarity in shape between the parent material (Figure 4a) and the dispersed nanosheet may indicate that, in some cases, BNNSs can be exfoliated without breakage events. Dynamic light scattering (DLS) was also utilized to measure the size (hydrodynamic radius) distribution of BNNSs (Figures S3-S4). From the DLS data, the number-

average hydrodynamic radius for the dispersed BNNSs is 204 nm and the maximum value is 900 nm; these values compare quite well against the TEM images in Figure 4, given that hydrodynamic radius is typically smaller than the apparent lateral size by a factor of at least 2. Further sonication of this dispersion (0.5 hours, 1 hour) indicates breakage of the largest nanosheets; details are shown in Supporting Information.

In the case of MoS_2 nanosheets, irregular edges are observed and the typical sheet size is ~500 nm (Figure 5c). The WS_2 nanosheets exhibit straight edges with a "folded paper" appearance, and the typical sheet size is ~400 nm (Figure 5e). The number of layers in the observed nanosheet was determined by the magnified view of the sheet edges (Figure 5b, 5d, and 5f).The number of visible, distinct layers at the edge confirm that the nanosheets are 2-5 layers thick, which is consistent with prior work in stable nanosheet dispersions. Unusually, the BNNSs and WS_2 nanosheets show distinct, paper-like folds. In contrast, TEM images of graphene in prior studies show that graphene has more tendencies to form irregular wrinkles and folds.[52,53] Some of these features (e.g., shape) are reflective of differences in parent material morphology; however, the straight edges and folds may indicate differences in bending moduli and sonication response.

The effect of initial parent material concentration on the final concentration of inorganic nanosheets was investigated. In all these experiments, 10 mg mL^{-1} PVP concentration was used. The final dispersed nanomaterial concentration increases with the initial parent material concentration, as shown in Figure 6. This is in agreement with our prior work on pristine graphene produced from graphite.[22,53,54] This relationship between nanomaterial concentration and parent material concentration has implications for the scalability of sonication-based methods; at low initial material concentrations, there is a linear relationship describing the yield

of nanosheets from the raw material. At higher initial material concentrations, this trend may plateau due to limitations in sonication effectiveness caused by the additional material and increased viscosity. (This same data is available with error estimates in Figure S5.) The dependence of the supernatant concentration on the PVP concentration was also investigated. The concentration of parent material was taken as 20 mg mL^{-1}. Figure 7 shows the nanomaterial concentration as a function of PVP concentration. Again, at higher PVP concentrations, there is a plateau in the as-obtained nanosheet concentration; similarly, this is likely due to increases in viscosity and a resulting decrease in sonication efficiency. (This same data is available with error estimates in Figure S6.) A similar effect was observed for PVP-stabilized graphene.[52]

The PVP-stabilized nanomaterial dispersions were freeze dried and redispersed in water. All three freeze dried powders were redispersible in water without sonication, as demonstrated in Figure 8. The redispersed samples were centrifuged. In the case of BNNSs, no sedimentation was observed, whereas in the case of MoS_2 and WS_2, some visible sedimentation was observed. The absorption spectra of the PVP-stabilized nanomaterial dispersion before and after freeze-drying are plotted in Figure S7. The absorbance spectra indicate that the nanomaterial concentration decreases after the experiment by 25%, 42%, and 41% for BNNSs (Figure S7a), MoS_2 (Figure S7b), and WS_2 (Figure S7c), respectively. The redispersion shows that the PVP-nanosheet association remained through freeze-drying and prevented aggregation in those redispersed nanosheets. However, the recovery of the dispersed nanosheets is only partial, indicating that some aggregation did occur, in contrast to graphene which showed complete redispersion.[55]

In addition to aqueous dispersions of inorganic nanomaterials (BNNSs, MoS_2, and WS_2) stabilized by PVP, we also investigated the applicability of PVP as a dispersant in organic

solvents. We find that PVP successfully stabilizes BNNSs, MoS_2, and WS_2 in methanol, ethanol, isopropanol, chloroform, DMF, DMSO, and NMP at 10 mg mL^{-1} PVP concentration and 20 mg mL^{-1} parent material concentration. The supernatant concentration and the extinction coefficient (BNNSs at 350 nm, MoS_2 at 674 nm and WS_2 630 nm) in the organic solvents are reported in Table S2 and Figures S8-S14.

3.2. Simulation of polymer interaction with nanosheets

The non-covalent interactions between PVP and isolated BNNS in water medium were investigated in this work using MD simulations. We varied the distance between the center of mass of the PVP molecule and the nanosheet surface. The interaction between the PVP molecule and the BNNS was monitored by keeping track of the shortest distance between any atom of the PVP chain and the BNNS. For the three systems studied, this initial shortest distance ($d_{initial}$) values are: 8.15 *Å*, 18.25 *Å* and 33.4 *Å*; also see Figure 1a for initial structure of the PVP chain after the equilibration stage. Given that the cut-off distance for calculation of interactions is 12 Å, only the PVP chain in the first system interacts directly with the BNNS, and even in that case, this interaction between the PVP chain and the BNNS will be of a small magnitude. The shortest distance between the BNNS and the PVP chain is plotted as a function of time in Figure 9 for all three cases. It is seen that for the first two cases, i.e., when the initial distance between PVP chain and the BNNS is 8.15 *Å* or 18.25 *Å,* after some initial exploring, the PVP molecule was observed to move directly towards the BNNS. Furthermore, in both cases, it is seen that once a part of the chain approaches within a distance of 3 *Å* of the BNNS, this distance of closest approach between the two molecules is maintained for the rest of the simulation duration. For the third case (initial BNNS-PVP separation distance, $d_{initial}$ = 33.4 *Å*), it is seen that the PVP chain approaches the surface but not in a monotonic fashion. As would be characteristic for

random thermal motion of the chain, the distance between the PVP chain and the BNNS shows oscillatory behavior. However, over a longer period of time, the chain does gradually move towards the surface and eventually, a part of the chain approaches within 3 *Å* of the BNNS at the simulation time of around 20 *ns*. Interestingly, similar to the other two cases, once a part of the PVP chain comes in close proximity with the BNNS, the distance of closest approach between the two molecules is maintained for the rest of the simulation duration. In summary, the PVP migrated to the nanosheet surface and remained there in a kinetically trapped, physisorbed state in all three cases.

3.3. Crumpling of inorganic nanosheets

Recently, we showed that simple industrial spray drying can induce the crumpling of pristine graphene nanosheets.[33] In this process, micron-sized droplets are produced by using an atomizer; the droplets are then evaporated by a hot air stream to produce a dry powder. The dry powders are settled by a cyclone separator, and close inspection shows a smooth crumpled morphology. This process is rapid and scalable; these nanosheet dispersions can be spray-dried more rapidly than they can be produced.

Here, we apply this spray drying technique to BNNSs, MoS_2, and WS_2 dispersions to investigate the universal use of this process; we demonstrate for the first time that inorganic nanosheets can be crumpled. The dispersions were spray dried at 220°C and 60 psi. Figures 10a, 10b, and 10c depict the first-ever images of crumpled BNNSs, MoS_2, and WS_2, respectively. The inset shows a magnified view of the crumpled sheets. The morphology of the crumpled particles indicates that all three nanosheets deformed due to capillary forces exerted on them during droplet evaporation. Our group is currently studying the mechanism of the nanosheets deformation. High surface tension at the water-air interface induces buckling of the nanosheets.

Complete removal of the water results in 3D particles with a dimpled appearance on the surface. The typical particle size for the samples was 1-2 μm, and the as-observed particle size distribution appears to be fairly narrow. Additional SEM images of crumpled nanosheets are shown in Figure S15.

When these images are compared against our earlier work on crumpled pristine graphene and graphene oxide, we note certain similarities.[33] In particular, the crumpled appearance of the inorganic nanosheets shows a smooth appearance with large dimples; this is similar to the prior images of pristine graphene. This implies that the deformation mechanism is similar for both pristine graphene and these inorganic nanosheets. This crumpling mechanism was detailed in our earlier work with pristine graphene. The schematic of the proposed mechanism is illustrated in Figure S16, which shows a droplet of the nanosheet dispersion coming out from the atomizer and flowing through the spray drier in the hot air stream. During evaporation, the nanosheets concentrate at the surface of the droplet and form a continuous shell. The final crumpled morphology can be explained by elastic shell deformation theory.[56,57] As the water evaporates, capillary forces compress the shell; consequently, the nanosheet shell yields and buckles due to strong compression forces, in accordance with elastic shell deformation theory.[56-58] This buckled, dimpled appearance is distinct from that shown by crumpled graphene oxide, which displays a tightly wrinkled appearance because of functional groups, surface defects, and localized bending.[29,59,60] Again this process, particularly the balance between convective and diffusive mass transfer, is discussed in detail in the previous report.[33]

Interestingly, the images in Figure 10 bear remarkable similarity to those seen in Doshi *et al.*'s simulations of elastic shells undergoing isotropic volume reduction.[33,61] Depending on the moduli of the shell itself, dimpled structures form as the interior volume is reduced. If the

nanosheets form a near-enclosed shell for the final stages of evaporation, these simulations are a strong indicator of the physical mechanisms of buckling and dimple formation.

4. Conclusions

We demonstrate a simple and effective technique to disperse inorganic layered nanomaterials in a range of solvents, using PVP as dispersant. These nanosheets include BNNSs, MoS_2 nanosheets, and WS_2 nanosheets. The aqueous dispersions of the inorganic nanomaterials in presence of polymer were stable after centrifugation. The aqueous dispersions also showed aggregation-resistance even after freeze-drying and redispersion. The morphology (lateral size, number of layers, and hydrodynamic radius) of the nanosheets was measured by TEM, SEM, and DLS. Such dispersions are useful for preparation of both nanosheet-based films and dielectric polymer nanocomposites.

Our simulations show that the PVP chain initially exhibits random thermal motion in water and eventually approaches within the range of interaction with the BNNS. The three simulations indicate that once the chain gets within close proximity of the BNNS, the separation distance between the two does not increase. This observation suggests a strong affinity between the PVP chain and the BNNS in the presence of water. We note that similar affinity between cello-oligosaccharide oligomers and cellulose crystal surface was observed in prior MD simulations work.[62] Future work will consist of determination of the free energy profile for the separation of the PVP chain from the BNNS in water solvent. Such free energy calculations will yield detailed information on the mechanism of PVP adsorption on the BNNS surface.

Furthermore, the aqueous dispersions were spray dried to form a 3D crumpled nanosheet powder. The SEM images of the first-ever crumpled nanosheets confirm the 3D morphology of the final product. Such techniques can be used to produce crumpled nanosheet powders with

high surface area and aggregation resistance, suitable for dielectric composites and energy storage electrodes.

Acknowledgements

We acknowledge Dr. Sriya Das, Fahmida Irin, and Charles Brandon Sweeney for productive suggestions. TEM and SEM were performed at the TTU Imaging Center (funded by NSF MRI 04-511) with help from Dr. Mark J. Grimson, Dr. Callum Hetherington, Mary Catherine Hastert, and Dr. Lauren Gollahon. Size characterization was conducted in the Materials Characterization Center with the support of Dr. Juliusz Warzywoda and Dr. Al Sacco of TTU. We would like to thank Steve Graham from Buchi for setting up spray dryer. Funding was provided by a 2014 DuPont Young Faculty Award and the U.S. National Science Foundation (NSF) under CAREER award CMMI-1253085.

LIST OF FIGURES

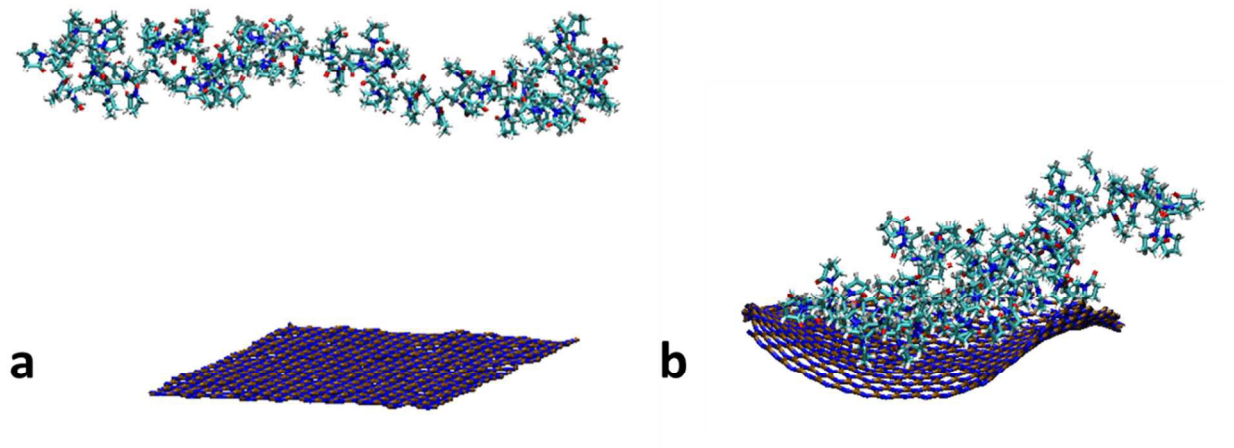

Figure 1. (a) Initial and (b) end configuration of the system with $d_{initial} = 33.4\ \mathring{A}$.

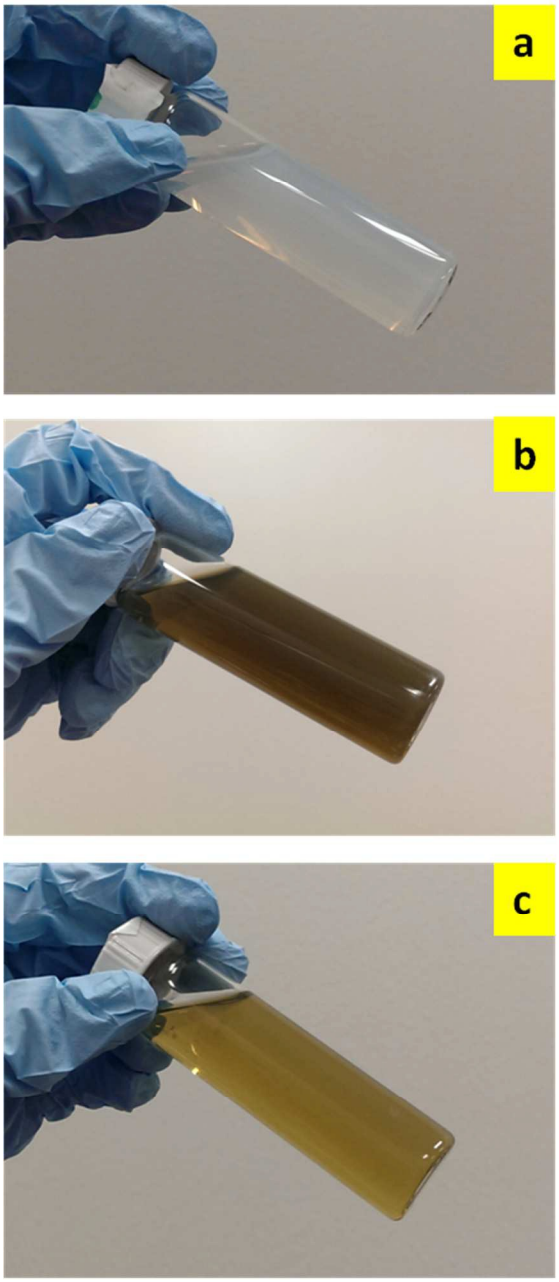

Figure 2. Images of PVP-stabilized aqueous dispersions of (a) BNNSs, (b) MoS_2, and (c) WS_2

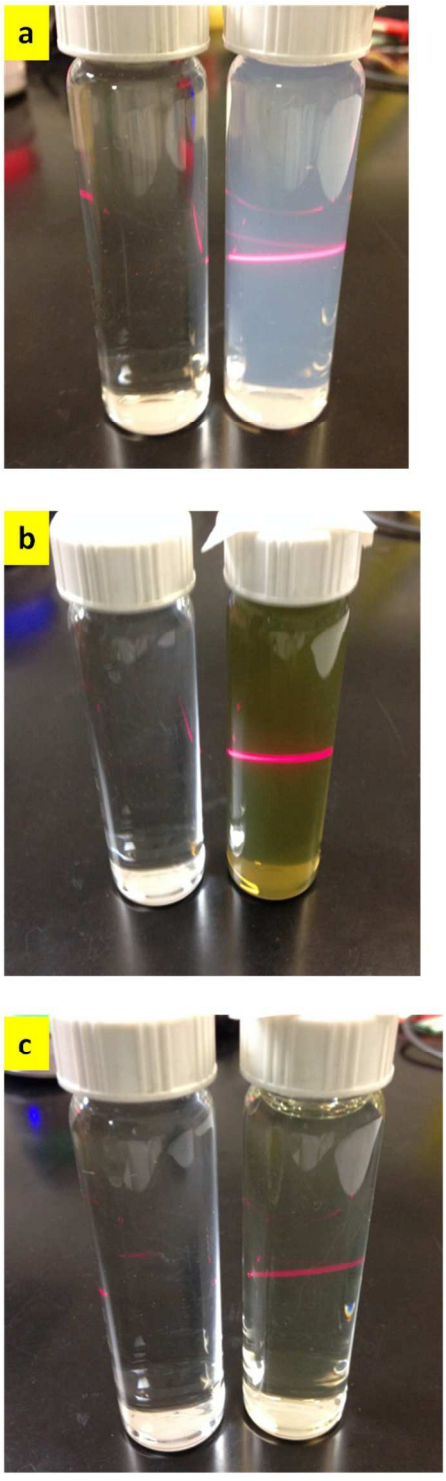

Figure 3. Tyndall effect demonstrated for PVP-stabilized aqueous dispersions of (a) BNNSs, (b) MoS_2, and (c) WS_2

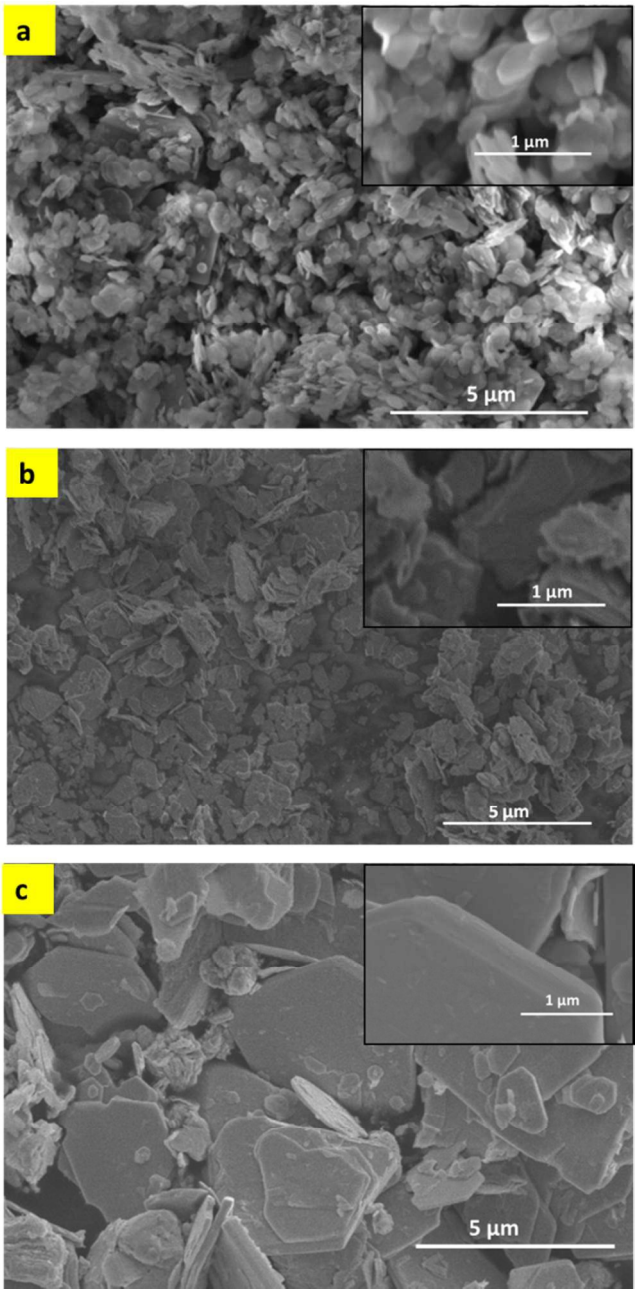

Figure 4. SEM images of the parent bulk material (a) BN, (b) MoS_2, and (c) WS_2

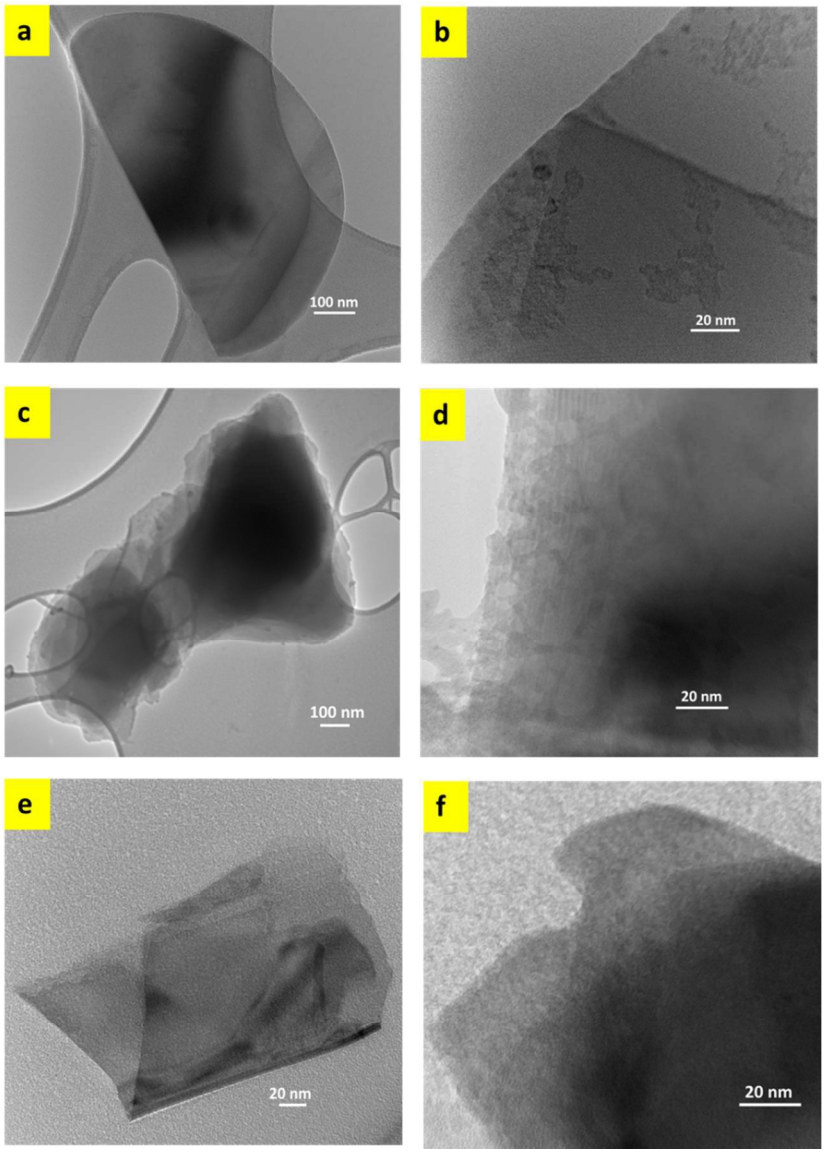

Figure 5. HRTEM images of: (a, b) BNNSs, (c, d) MoS_2 nanosheets, (e, f) WS_2 nanosheets. Images in (a, c, e) show folded BNNS, MoS_2, and WS_2 sheets. Images in (b, d, f) show sheet edges of the dispersed nanosheets; sheet edges indicate that the nanosheets are 2-5 layers thick.

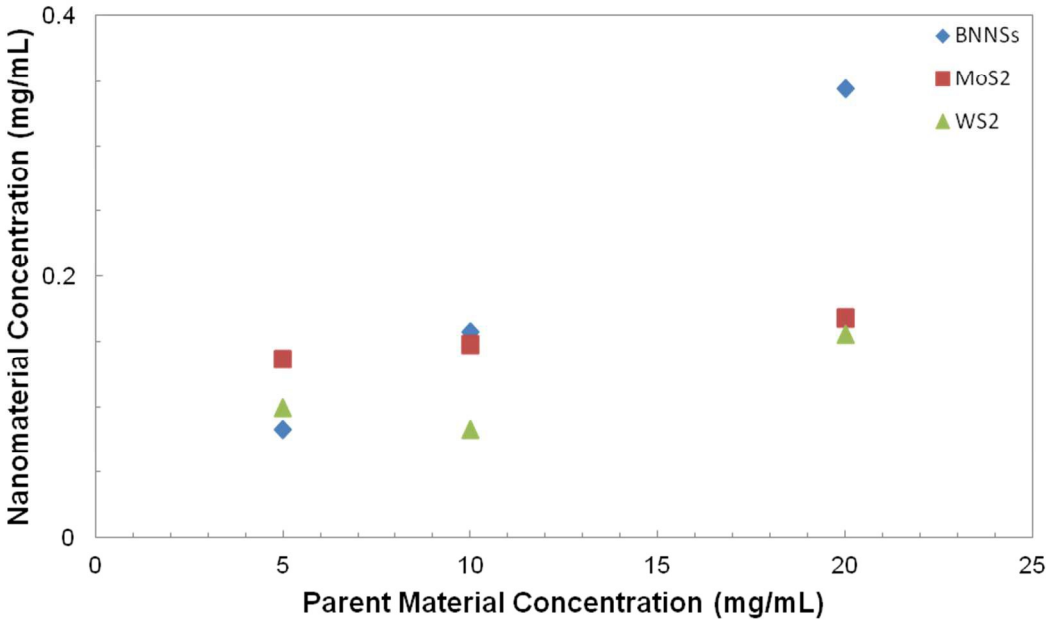

Figure 6. The final concentration of dispersed, stable nanosheets increases with the initial concentration of the parent material in the sonication vial (PVP concentration is 10 mg/mL).In some cases, a plateau is reached, possibly due to increased viscosity and decreased sonication efficiency.

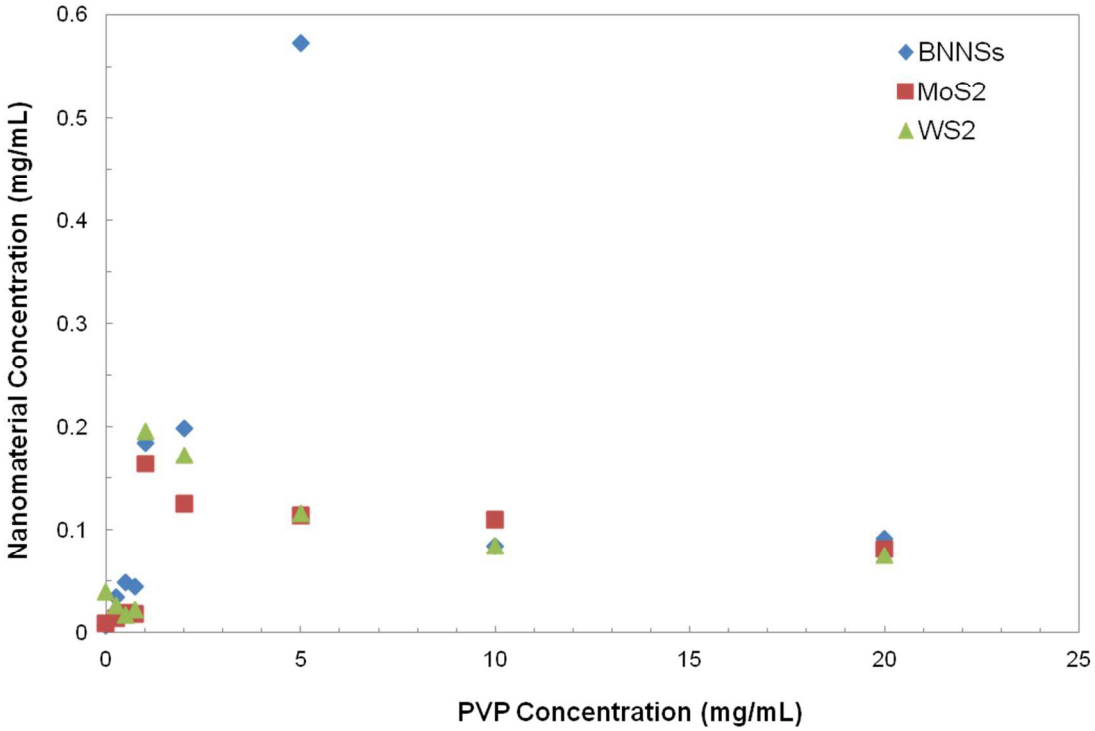

Figure 7. The effect of increasing PVP concentration on the final nanomaterial concentration in the dispersion is demonstrated (20 mg/mL parent material in sonication vial). Again, there is a decrease and a plateau at higher PVP concentrations; this may be due to increases in viscosity and decreasing sonication efficiency.

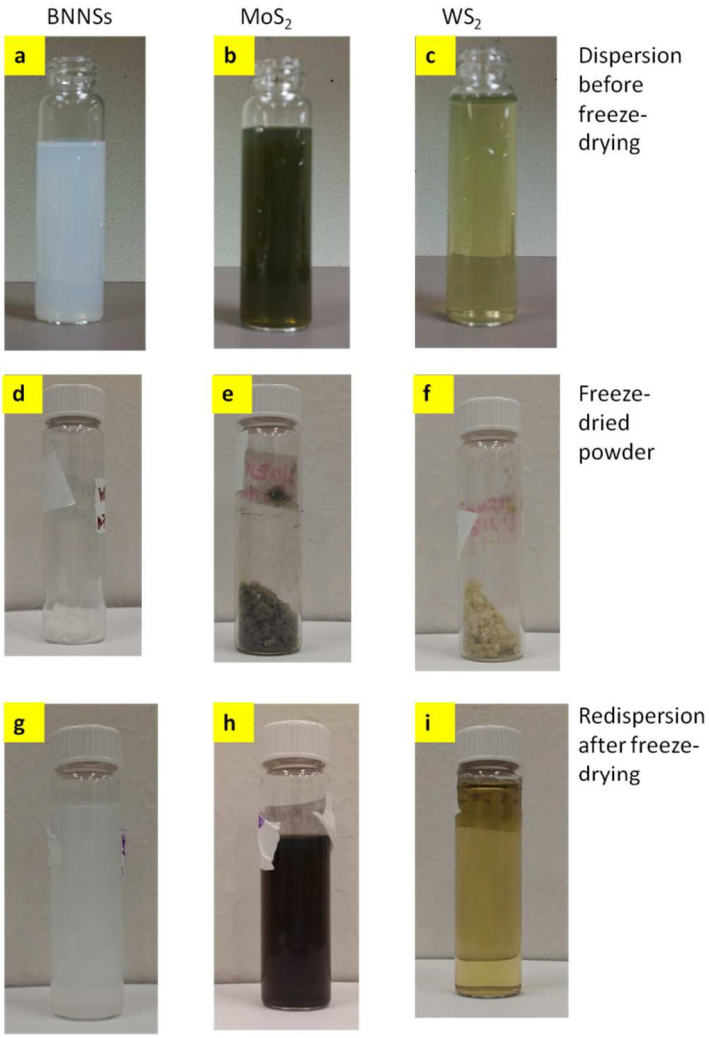

Figure 8. Freeze-dried, PVP-stabilized (a) BNNSs, (c) MoS_2, (e) WS_2 powders and the corresponding redispersed (b) BNNSs, (d) MoS_2, (f) WS_2 in water. The freeze dried powders were then dispersed in water without sonication for (g) BNNSs, (h) MoS_2, (i) WS_2, yielding partial recovery of the initial dispersion.

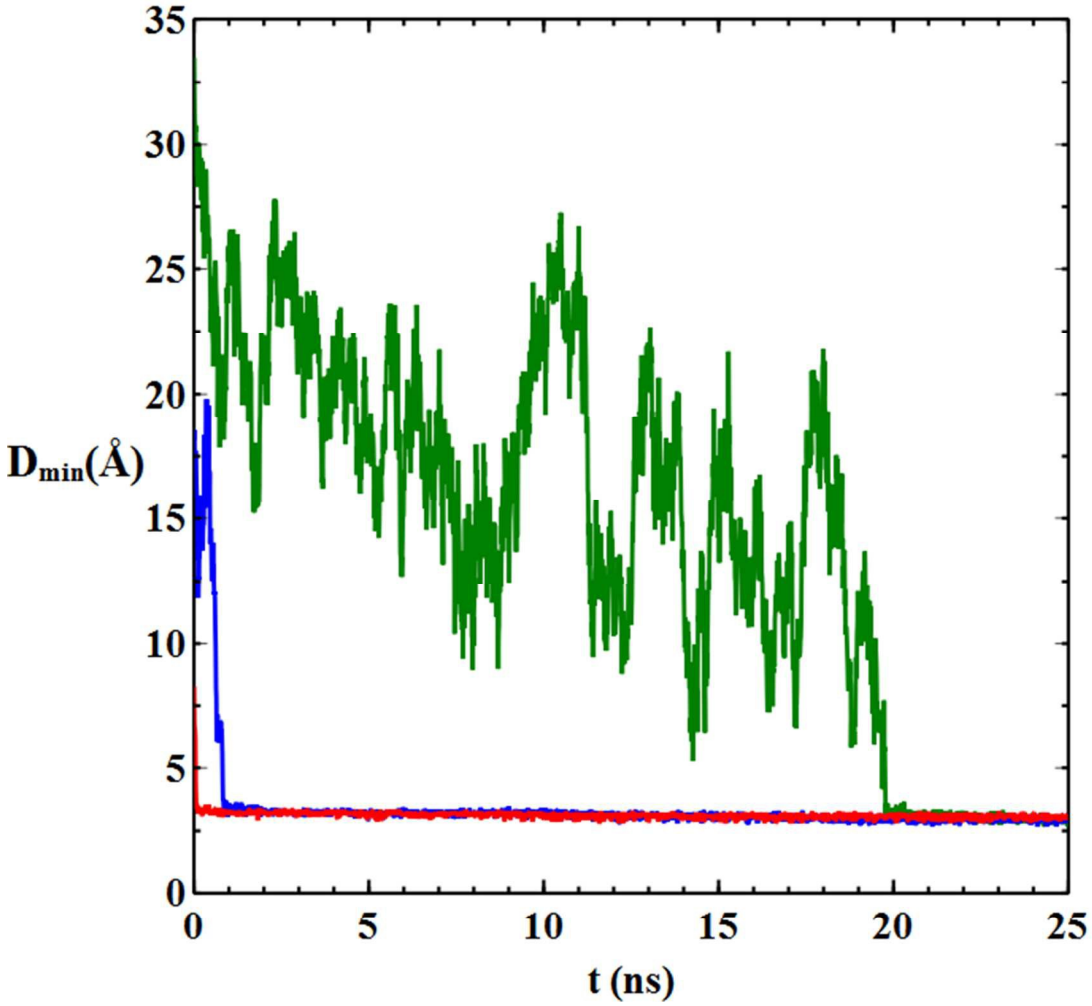

Figure 9. The shortest distance of the *PVP* chain from the surface of the *BNNS*. Initial distances are shown as red (8.15 *Å*), blue (18.25 *Å*), and green 33.4 *Å*.

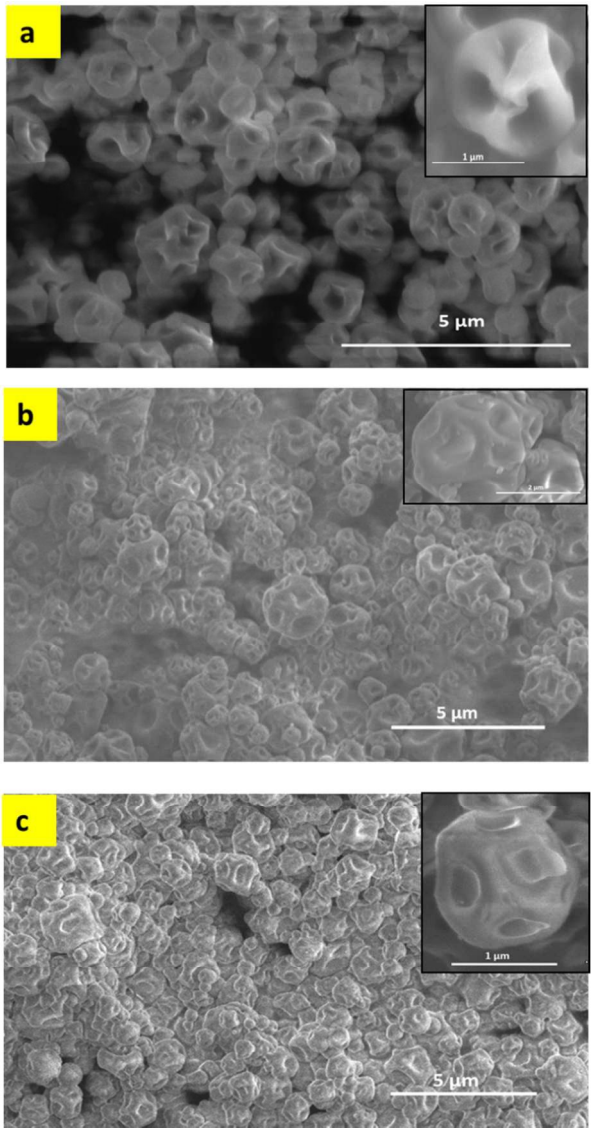

Figure 10. SEM images of crumpled nanosheets collected from the spray dryer; (a) BNNSs, (b) MoS_2, and (c) WS_2. The inset shows a magnified view of the crumpled nanosheets. The dimples indicate the formation of hollow shells with sides buckled in; this has been observed in the prior literature on elastic powder shells formed during spray drying of other particulate dispersions as well.

REFERENCES

(1) Tenne, R.; Homyonfer, M.; Feldman, Y. Nanoparticles of layered compounds with hollow cage structures (inorganic fullerene-like structures). *Chemistry of materials* **1998**, *10*, 3225-3238.

(2) Margolin, A.; Rosentsveig, R.; Albu-Yaron, A.; Popovitz-Biro, R.; Tenne, R. Study of the growth mechanism of WS2 nanotubes produced by a fluidized bed reactor. *Journal of Materials Chemistry* **2004**, *14*, 617-624.

(3) Rosentsveig, R.; Margolin, A.; Feldman, Y.; Popovitz-Biro, R.; Tenne, R. Bundles and foils of WS2 nanotubes. *Applied Physics A* **2002**, *74*, 367-369.

(4) Kaplan-Ashiri, I.; Tenne, R. Mechanical properties of WS2 nanotubes. *Journal of Cluster Science* **2007**, *18*, 549-563.

(5) Ishii, T.; Sato, T.; Sekikawa, Y.; Iwata, M. Growth of whiskers of hexagonal boron nitride. *Journal of Crystal Growth* **1981**, *52, Part 1*, 285-289.

(6) Seifert, G.; Terrones, H.; Terrones, M.; Jungnickel, G.; Frauenheim, T. Structure and electronic properties of MoS2 nanotubes. *Physical Review Letters* **2000**, *85*, 146-149.

(7) Lin, Y.; Williams, T. V.; Connell, J. W. Soluble, Exfoliated Hexagonal Boron Nitride Nanosheets. *Journal of Physical Chemistry Letters* **2010**, *1*, 277-283.

(8) Golberg, D.; Bando, Y.; Huang, Y.; Terao, T.; Mitome, M.; Tang, C.; Zhi, C. Boron Nitride Nanotubes and Nanosheets. *Acs Nano* **2010**, *4*, 2979-2993.

(9) Lin, Y.; Connell, J. W. Advances in 2D boron nitride nanostructures: nanosheets, nanoribbons, nanomeshes, and hybrids with graphene. *Nanoscale* **2012**, *4*, 6908-6939.

(10) Zhu, H.; Li, Y.; Fang, Z.; Xu, J.; Cao, F.; Wan, J.; Preston, C.; Yang, B.; Hu, L. Highly Thermally Conductive Papers with Percolative Layered Boron Nitride Nanosheets. *ACS Nano* **2014**, *8*, 3606-3613.

(11) Wang, Q. H.; Kalantar-Zadeh, K.; Kis, A.; Coleman, J. N.; Strano, M. S. Electronics and optoelectronics of two-dimensional transition metal dichalcogenides. *Nature Nanotechnology* **2012**, *7*, 699-712.

(12) Kuc, A.; Zibouche, N.; Heine, T. Influence of quantum confinement on the electronic structure of the transition metal sulfide T S 2. *Physical Review B* **2011**, *83*, 245213.

(13) Mak, K. F.; Lee, C.; Hone, J.; Shan, J.; Heinz, T. F. Atomically thin MoS 2: a new direct-gap semiconductor. *Physical Review Letters* **2010**, *105*, 136805.

(14) Splendiani, A.; Sun, L.; Zhang, Y.; Li, T.; Kim, J.; Chim, C.-Y.; Galli, G.; Wang, F. Emerging photoluminescence in monolayer MoS2. *Nano letters* **2010**, *10*, 1271-1275.

(15) Mak, K. F.; He, K.; Shan, J.; Heinz, T. F. Control of valley polarization in monolayer MoS2 by optical helicity. *Nature Nanotechnology* **2012**, *7*, 494-498.

(16) Aruchamy, A.: *Photoelectrochemistry and photovoltaics of layered semiconductors*; Springer, 1992; Vol. 14.

(17) Guardia, L.; Paredes, J. I.; Rozada, R.; Villar-Rodil, S.; Martinez-Alonso, A.; Tascon, J. M. D. Production of aqueous dispersions of inorganic graphene analogues by exfoliation and stabilization with non-ionic surfactants. *RSC Advances* **2014**, *4*, 14115-14127.

(18) Coleman, J. N.; Lotya, M.; O'Neill, A.; Bergin, S. D.; King, P. J.; Khan, U.; Young, K.; Gaucher, A.; De, S.; Smith, R. J.; Shvets, I. V.; Arora, S. K.; Stanton, G.; Kim, H.-Y.; Lee, K.; Kim, G. T.; Duesberg, G. S.; Hallam, T.; Boland, J. J.; Wang, J. J.; Donegan, J. F.; Grunlan, J. C.; Moriarty, G.; Shmeliov, A.; Nicholls, R. J.; Perkins, J. M.; Grieveson, E. M.; Theuwissen, K.; McComb, D. W.; Nellist, P. D.; Nicolosi, V. Two-Dimensional Nanosheets Produced by Liquid Exfoliation of Layered Materials. *Science* **2011**, *331*, 568-571.

(19) Smith, R. J.; King, P. J.; Lotya, M.; Wirtz, C.; Khan, U.; De, S.; O'Neill, A.; Duesberg, G. S.; Grunlan, J. C.; Moriarty, G.; Chen, J.; Wang, J.; Minett, A. I.; Nicolosi, V.; Coleman, J. N. Large-Scale

Exfoliation of Inorganic Layered Compounds in Aqueous Surfactant Solutions. *Advanced Materials* **2011**, *23*, 3944-+.

(20) Zhi, C.; Bando, Y.; Tang, C.; Kuwahara, H.; Golberg, D. Large-Scale Fabrication of Boron Nitride Nanosheets and Their Utilization in Polymeric Composites with Improved Thermal and Mechanical Properties. *Advanced Materials* **2009**, *21*, 2889-+.

(21) Warner, J. H.; Ruemmeli, M. H.; Bachmatiuk, A.; Buechner, B. Atomic Resolution Imaging and Topography of Boron Nitride Sheets Produced by Chemical Exfoliation. *Acs Nano* **2010**, *4*, 1299-1304.

(22) Wajid, A. S.; Das, S.; Irin, F.; Ahmed, H. S. T.; Shelburne, J. L.; Parviz, D.; Fullerton, R. J.; Jankowski, A. F.; Hedden, R. C.; Green, M. J. Polymer-stabilized graphene dispersions at high concentrations in organic solvents for composite production. *Carbon* **2012**, *50*, 526-534.

(23) Ma, P.; Spencer, J. T. Non-covalent stabilization and functionalization of boron nitride nanosheets (BNNSs) by organic polymers: formation of complex BNNSs-containing structures. *Journal of Materials Science* **2014**, 1-11.

(24) Jeong Won, K.; Ho Jung, H. Comparison of C 60 encapsulations into carbon and boron nitride nanotubes. *J. Phys.: Condens. Matter* **2004**, *16*, 3901.

(25) Nasrabadi, A. T.; Foroutan, M. Interactions between Polymers and Single-Walled Boron Nitride Nanotubes: A Molecular Dynamics Simulation Approach. *The Journal of Physical Chemistry B* **2010**, *114*, 15429-15436.

(26) Saikat, M.; Gowtham, S.; Ralph, H. S.; Ravindra, P.; Shashi, P. K. Theoretical study of physisorption of nucleobases on boron nitride nanotubes: a new class of hybrid nano-biomaterials. *Nanotechnology* **2010**, *21*, 165703.

(27) Gou, G.; Pan, B.; Shi, L. Noncovalent Functionalization of BN Nanotubes with Perylene Derivative Molecules: An ab Initio Study. *ACS Nano* **2010**, *4*, 1313-1320.

(28) Ding, N.; Chen, X.; Wu, C.-M. L.; Li, H. Adsorption of nucleobase pairs on hexagonal boron nitride sheet: hydrogen bonding versus stacking. *Physical Chemistry Chemical Physics* **2013**, *15*, 10767-10776.

(29) Luo, J.; Jang, H. D.; Sun, T.; Xiao, L.; He, Z.; Katsoulidis, A. P.; Kanatzidis, M. G.; Gibson, J. M.; Huang, J. Compression and Aggregation-Resistant Particles of Crumpled Soft Sheets. *Acs Nano* **2011**, *5*, 8943-8949.

(30) Sohn, K.; Na, Y. J.; Chang, H.; Roh, K.-M.; Jang, H. D.; Huang, J. Oil absorbing graphene capsules by capillary molding. *Chemical Communications* **2012**, *48*, 5968-5970.

(31) Luo, J.; Zhao, X.; Wu, J.; Jang, H. D.; Kung, H. H.; Huang, J. Crumpled Graphene-Encapsulated Si Nanoparticles for Lithium Ion Battery Anodes. *Journal of Physical Chemistry Letters* **2012**, *3*, 1824-1829.

(32) Luo, J.; Jang, H. D.; Huang, J. Effect of Sheet Morphology on the Scalability of Graphene-Based Ultracapacitors. *Acs Nano* **2013**, *7*, 1464-1471.

(33) Parviz, D.; Metzler, S. D.; Das, S.; Irin, F.; Green, M. J. Tailored crumpling and unfolding of spray-dried pristine graphene and graphene oxide sheets *Small* **2014**, *accepted*.

(34) Tersoff, J. New empirical approach for the structure and energy of covalent systems. *Phys. Rev. B: Condens. Matter Mater. Phys.* **1988**, *37*, 6991-7000.

(35) Jorgensen, W. L.; Chandrasekhar, J.; Madura, J. D.; Impey, R. W.; Klein, M. L. Comparison of simple potential functions for simulating liquid water. *The Journal of Chemical Physics* **1983**, *79*, 926-935.

(36) Ryckaert, J.-P.; Ciccotti, G.; Berendsen, H. J. C. Numerical integration of the cartesian equations of motion of a system with constraints: molecular dynamics of n-alkanes. *J. Comput. Phys.* **1977**, *23*, 327-341.

(37) Wang, J.; Wang, W.; Kollman, P. A.; Case, D. A. Automatic atom type and bond type perception in molecular mechanical calculations. *J. Mol. Graphics Modell.* **2006**, *25*, 247-260.

(38) Wang, J.; Wolf, R. M.; Caldwell, J. W.; Kollman, P. A.; Case, D. A. Development and testing of a general amber force field. *J. Comput. Chem.* **2004**, *25*, 1157-1174.

(39) Mayo, S. L.; Olafson, B. D.; Goddard, W. A. DREIDING: a generic force field for molecular simulations. *J. Phys. Chem.* **1990**, *94*, 8897-8909.

(40) Jakalian, A.; Bush, B. L.; Jack, D. B.; Bayly, C. I. Fast, efficient generation of high-quality atomic charges. AM1-BCC model: I. Method. *J. Comput. Chem.* **2000**, *21*, 132-146.

(41) Jakalian, A.; Jack, D. B.; Bayly, C. I. Fast, efficient generation of high-quality atomic charges. AM1-BCC model: II. Parameterization and validation. *J. Comput. Chem.* **2002**, *23*, 1623-1641.

(42) Hod, O. Graphite and Hexagonal Boron-Nitride have the Same Interlayer Distance. Why? *J. Chem. Theory Comput.* **2012**, *8*, 1360-1369.

(43) Hockney R.W ; J.W, E.: *Computer Simulation Using Particles* CRC Press: New York, 1989.

(44) Shinoda, W.; Shiga, M.; Mikami, M. Rapid estimation of elastic constants by molecular dynamics simulation under constant stress. *Physical Review B* **2004**, *69*, 134103.

(45) Plimpton, S. Fast Parallel Algorithms for Short-Range Molecular Dynamics. *J. Comput. Phys.* **1995**, *117*, 1-19.

(46) Lu, F.; Wang, F.; Gao, W.; Huang, X.; Zhang, X.; Li, Y. Aqueous soluble boron nitride nanosheets via anionic compound-assisted exfoliation. *Materials Express* **2013**, *3*, 144-150.

(47) Lu, P.; Wu, X.; Guo, W.; Zeng, X. C. Strain-dependent electronic and magnetic properties of MoS2 monolayer, bilayer, nanoribbons and nanotubes. *Physical Chemistry Chemical Physics* **2012**, *14*, 13035-13040.

(48) Liu, Z.; Suenaga, K.; Wang, Z.; Shi, Z.; Okunishi, E.; Iijima, S. Identification of active atomic defects in a monolayered tungsten disulphide nanoribbon. *Nat Commun* **2011**, *2*, 213.

(49) Yuan, Y.-J.; Yu, Z.-T.; Liu, X.-J.; Cai, J.-G.; Guan, Z.-J.; Zou, Z.-G. Hydrogen Photogeneration Promoted by Efficient Electron Transfer from Iridium Sensitizers to Colloidal MoS2 Catalysts. *Sci. Rep.* **2014**, *4*, 4045.

(50) Yu, J.; Huang, X.; Wu, C.; Wu, X.; Wang, G.; Jiang, P. Interfacial modification of boron nitride nanoplatelets for epoxy composites with improved thermal properties. *Polymer* **2012**, *53*, 471-480.

(51) Paton, K. R.; Varrla, E.; Backes, C.; Smith, R. J.; Khan, U.; O'Neill, A.; Boland, C.; Lotya, M.; Istrate, O. M.; King, P.; Higgins, T.; Barwich, S.; May, P.; Puczkarski, P.; Ahmed, I.; Moebius, M.; Pettersson, H.; Long, E.; Coelho, J.; O'Brien, S. E.; McGuire, E. K.; Sanchez, B. M.; Duesberg, G. S.; McEvoy, N.; Pennycook, T. J.; Downing, C.; Crossley, A.; Nicolosi, V.; Coleman, J. N. Scalable production of large quantities of defect-free few-layer graphene by shear exfoliation in liquids. *Nat Mater* **2014**, *13*, 624-630.

(52) Wajid, A. S.; Das, S.; Irin, F.; Ahmed, H. S. T.; Shelburne, J. L.; Parviz, D.; Fullerton, R. J.; Jankowski, A. F.; Hedden, R. C.; Green, M. J. Polymer-stabilized graphene dispersions at high concentrations in organic solvents for composite production (vol 50, pg 526, 2012). *Carbon* **2012**, *50*, 2065-2065.

(53) Das, S.; Irin, F.; Ahmed, H. S. T.; Cortinas, A. B.; Wajid, A. S.; Parviz, D.; Jankowski, A. F.; Kato, M.; Green, M. J. Non-covalent functionalization of pristine few-layer graphene using triphenylene derivatives for conductive poly (vinyl alcohol) composites. *Polymer* **2012**, *53*, 2485-2494.

(54) Parviz, D.; Das, S.; Ahmed, H. S. T.; Irin, F.; Bhattacharia, S.; Green, M. J. Dispersions of Non-Covalently Functionalized Graphene with Minimal Stabilizer. *ACS Nano* **2012**, *6*, 8857-8867.

(55) Wajid, A. S.; Das, S.; Irin, F.; Ahmed, H. S. T.; Shelburne, J. L.; Parviz, D.; Fullerton, R. J.; Jankowski, A. F.; Hedden, R. C.; Green, M. J. Polymer-stabilized graphene dispersions at high concentrations in organic solvents for composite production. *Carbon* **2012**, *50*, 526-534.

(56) Tsapis, N.; Dufresne, E. R.; Sinha, S. S.; Riera, C. S.; Hutchinson, J. W.; Mahadevan, L.; Weitz, D. A. Onset of buckling in drying droplets of colloidal suspensions. *Physical Review Letters* **2005**, *94*.

(57) Bahadur, J.; Sen, D.; Mazumder, S.; Paul, B.; Bhatt, H.; Singh, S. G. Control of Buckling in Colloidal Droplets during Evaporation-Induced Assembly of Nanoparticles. *Langmuir* **2012**, *28*, 1914-1923.

(58) Chen, Y.; Guo, F.; Jachak, A.; Kim, S.-P.; Datta, D.; Liu, J.; Kulaots, I.; Vaslet, C.; Jang, H. D.; Huang, J.; Kane, A.; Shenoy, V. B.; Hurt, R. H. Aerosol Synthesis of Cargo-Filled Graphene Nanosacks. *Nano Letters* **2012**, *12*, 1996-2002.

(59) Ma, X.; Zachariah, M. R.; Zangmeister, C. D. Reduction of Suspended Graphene Oxide Single Sheet Nanopaper: The Effect of Crumpling. *Journal of Physical Chemistry C* **2013**, *117*, 3185-3191.

(60) Wang, W.-N.; Jiang, Y.; Biswas, P. Evaporation-Induced Crumpling of Graphene Oxide Nanosheets in Aerosolized Droplets: Confinement Force Relationship. *Journal of Physical Chemistry Letters* **2012**, *3*, 3228-3233.

(61) Sen, D.; Bahadur, J.; Mazumder, S.; Verma, G.; Hassan, P. A.; Bhattacharya, S.; Vijai, K.; Doshi, P. Nanocomposite silica surfactant microcapsules by evaporation induced self assembly: tuning the morphological buckling by modifying viscosity and surface charge. *Soft Matter* **2012**, *8*, 1955-1963.

(62) Peri, S.; Muthukumar, L.; Nazmul Karim, M.; Khare, R. Dynamics of cello-oligosaccharides on a cellulose crystal surface. *Cellulose* **2012**, *19*, 1791-1806.